

Effect of manganese concentration on physical properties of ZnS:Mn thin films prepared by chemical bath deposition

Abdelhak Jrad^{1,2} · Wafa Naffouti¹ · Tarek Ben Nasr¹ · Souad Ammar² · Najoua Turki-Kamoun¹

Received: 28 June 2016 / Accepted: 2 September 2016 / Published online: 9 September 2016
© Springer Science+Business Media New York 2016

Abstract ZnS:Mn thin films were grown by chemical bath deposition technique on glass substrates for different doping ratios $y = [\text{Mn}^{2+}]/[\text{Zn}^{2+}]$ ($y = 0, 6, 12$ and 18 at. %). Structural, morphological, optical and electrical properties were studied by X-ray diffraction (XRD), Fourier transform infrared spectroscopy (FTIR), scanning electron microscopy (SEM), UV–Vis–NIR spectrophotometry, spectrofluorimetry, Hall effect measurement. In fact, the XRD analysis showed that ZnS:Mn films were poorly crystalline. The average transmittance of all films was greater than 70 % in the visible range. The effect of Mn doping on refractive index, extinction coefficient and other optical parameters was also investigated. Measured electrical resistivity decreased slightly from 7.586×10^4 to $6.819 \times 10^4 \Omega \text{ cm}$ with increasing of doping concentration from 0 to 6 at. % then it increased again to achieve $16.73 \times 10^4 \Omega \text{ cm}$ for y equals to 18 at. %.

1 Introduction

II–VI compounds have attracted considerable attention owing to their interesting physical properties. Thus, ZnS is one of the most II–VI promising candidate that has extensive applications in optoelectronic devices [1]. It is widely used in solar cells [2], light emitting diodes [3], 2D

photonic crystal sensors [4], photocatalysis [5], infrared window and missile dome in defense applications [6]. Different techniques are used to synthesize ZnS thin films such as molecular beam epitaxy (MBE) [7], pulsed laser deposition (PLD) [8], close-spaced vacuum sublimation (CSVS) [9], RF magnetron sputtering [10], chemical vapor deposition (CVD) [11], metal organic chemical vapor deposition (MOCVD) [12], spray pyrolysis [13], successive ionic layer adsorption and reaction (SILAR) method [14], electrochemical deposition [15], and chemical bath deposition (CBD) [16]. Owing to its unique properties, CBD is considered as a simple and economic method as compared to other sophisticated techniques and it can be adapted easily for production of large-area thin films.

The intention of the present report is to investigate the effect of manganese doping on the structural, morphological, optical and electrical properties of ZnS thin films prepared by chemical bath deposition method in order to use it in optoelectronic devices.

2 Experimental details

2.1 Materials

ZnS:Mn films with 0, 6, 12 and 18 at. % of Mn were grown by CBD technique on glass substrates using zinc sulfate heptahydrate ($\text{ZnSO}_4 \cdot 7\text{H}_2\text{O}$), thiourea [$\text{SC}(\text{NH}_2)_2$], manganese sulfate monohydrate ($\text{MnSO}_4 \cdot \text{H}_2\text{O}$), ammonia (NH_4OH) and hydrazine hydrate ($\text{N}_2\text{H}_4 \cdot \text{H}_2\text{O}$). Bidistilled water was used in the entire synthesis. All prepared films include three successive layers, each of them being elaborated at 80 °C for a deposition time of 60 min. All used chemicals were supplied by Sigma-Aldrich Chemicals. The experimental process monitored for the elaboration of our

✉ Abdelhak Jrad
abdelhak.jrad@gmail.com

¹ Laboratoire de Physique de la Matière Condensée, Faculté des Sciences de Tunis El Manar, Université Tunis El Manar, 2092 Tunis, Tunisia

² CNRS UMR-7086, ITODYS, Université Paris Diderot, Sorbonne Paris Cité, 75013 Paris, France

samples was described with more details in previous study [16].

2.2 Characterization techniques

The crystalline quality of the prepared samples was examined by X-ray diffraction (XRD), using the copper radiation $K\alpha$ ($\lambda = 1.5418 \text{ \AA}$) in the 2θ range $10\text{--}90^\circ$ with a step size of 0.013° and a scan time per step of 2 s. Fourier transform infrared (FTIR) spectra were recorded using Perkin Elmer spectrometer from 400 to 4000 cm^{-1} . The morphology of the samples was carried out using Zeiss SUPRA 40 FEG-SEM. Optical transmittance and reflectance spectra were performed at room temperature in the wavelength range $[250\text{--}2500] \text{ nm}$ with a step size of 5 nm using Perkin Elmer lambda 950 spectrophotometer. Photoluminescence properties were investigated thanks to a Perkin Elmer LS55 spectrometer with an excitation wavelength of 300 nm. The electrical properties were recorded by ECOPIA Hall effect measurements system (HMS-3000 VER 3.51) at room temperature using standard field strength of about 0.55 Tesla.

3 Results and discussion

3.1 Structural analysis

The effect of manganese doping on the structure of zinc sulfide thin films is studied by XRD. The diffractograms (Fig. 1) depicts that ZnS:Mn thin films are characterized with a poorly cubic crystalline quality embedded in amorphous microstructure. No diffraction peaks corresponding to Mn or MnS were detected which indicates that Mn^{2+} ions may be incorporated successfully in the host lattice.

For further structural analysis, the crystallite size (D) is calculated using the following Scherrer's formula [17]:

$$D = \frac{0.9\lambda}{\beta \cos(\theta)} \quad (1)$$

where λ , θ and β are the X-ray wavelength, Bragg diffraction angle and the experimental full-width at half-maximum (FWHM), respectively. As seen from Table 1 and Fig. 2, the crystallite size varies in the range $[41.74\text{--}47.99] \text{ nm}$ which is in good agreement with the values reported by Ortiz-Hernández et al. [18].

The variation of microstrain (ε) is estimated from the following equation [19]:

$$\varepsilon = \frac{\beta \cos(\theta)}{4} \quad (2)$$

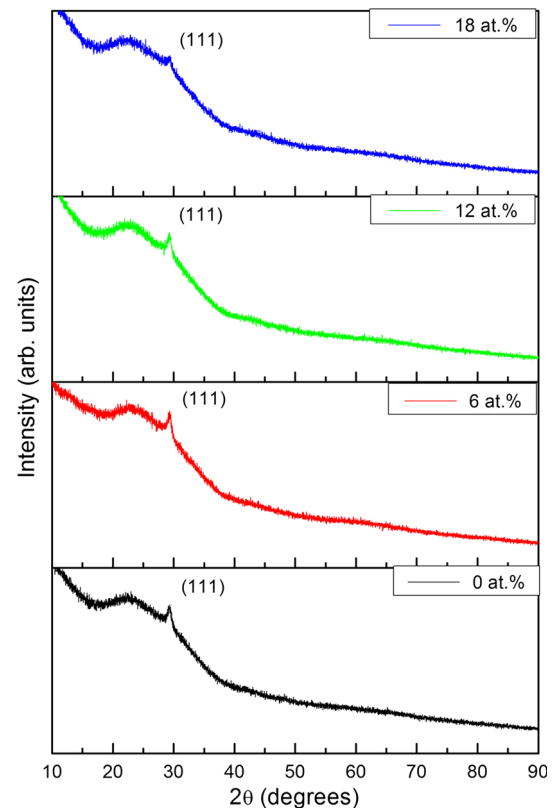


Fig. 1 X-ray diffraction patterns of ZnS:Mn thin films for different doping ratios

Table 1 The estimated values of crystallite size (D) and microstrain (ε) of ZnS:Mn thin films

y (at. %)	D (nm)	ε (%)
0	41.74	0.29
6	47.99	0.25
12	42.98	0.28
18	41.72	0.29

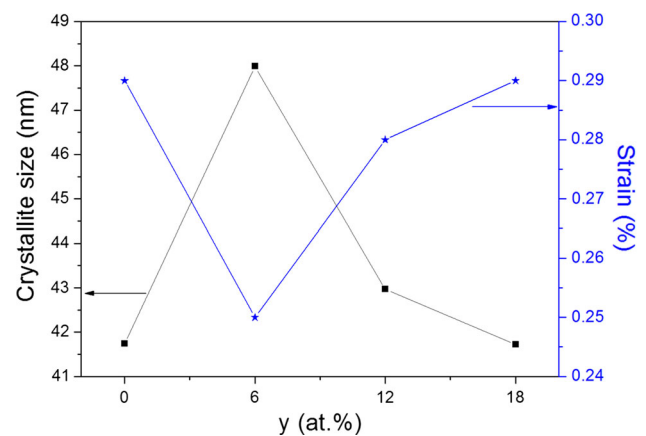


Fig. 2 The variation of crystallite size (D) and microstrain (ε) for different Mn concentrations

As depicted in Table 1 and Fig. 2, the highest crystallite size as well as the lowest microstrain are obtained for films doped at 6 at. % Mn concentration.

3.2 Fourier transforms infrared analysis

Figure 3 shows the FTIR spectra of ZnS:Mn films for various doping ratios. The as-prepared films contain several absorption peaks in the range 400–4000 cm⁻¹. Indeed, a strong and broad band located at 3436 cm⁻¹ can be observed. Furthermore, we can remark the presence of a strong and sharp band situated at 1636 cm⁻¹. Thus, both of them indicate the existence of hydroxyl ions and/or adsorbed water on the surface of the as-deposited films. The band observed at 3436 cm⁻¹ indicates O–H stretching vibration whereas the band located at 1636 cm⁻¹ is assigned to the H–O–H bending mode [6]. The bands located at around 2350 cm⁻¹ are attributed to the absorption peak of CO₂ [6]. The spectral bands in the range of 1000–1200 cm⁻¹ and 1300–1400 cm⁻¹ are the characteristics of S–O and Zn–O vibrational bands, respectively [20]. The absorption bands observed at 400–900 cm⁻¹ is related to the Zn–O vibration [6].

3.3 Morphological studies

The SEM micrographs of ZnS:Mn thin films doped at various Mn concentrations are displayed in Fig. 4. It is clearly seen that undoped sample micrograph shows significant agglomeration formed by nearly spherical particles with a diameter of around 200 nm. However, there are some cracks which are not practical. However, it is worth mentioning that there is a significant enhancement of the surface morphology after manganese doping. Indeed, for

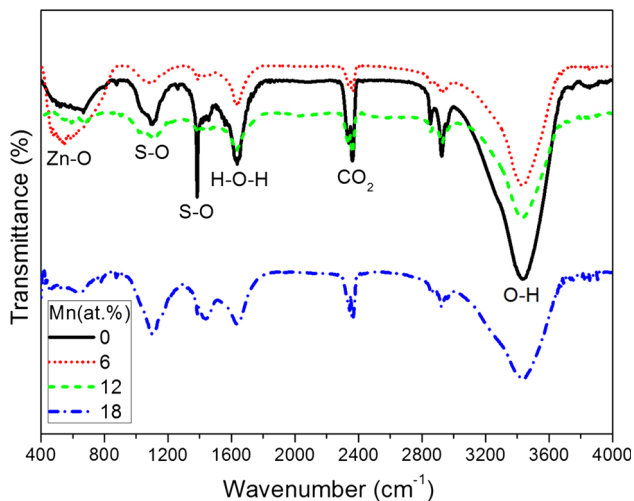


Fig. 3 FTIR spectra of ZnS:Mn thin films

sample doped at 6 at. % Mn, the surface becomes more homogenous and more compact without, practically, any cracks.

In order to have an idea about the film thickness, the cross-sectional SEM micrographs of undoped and ZnS: (6 at. % Mn) are displayed in Fig. 5. Thus, we note that the surface is dense, uniform and adherent to the substrate with an average thickness of around 200 nm.

3.4 Optical analysis

3.4.1 Transmittance and reflectance spectra

In order to investigate the effect of Mn doping on the optical properties of ZnS thin films, UV–Vis–NIR studies are performed. In fact, we remark, from Fig. 6, the presence of interference fringes in the visible region, which reflects the homogeneity of the grown films. Moreover, we can remark a slowly increase of transmittance in both visible and infrared regions after Mn doping. However, the reflectance spectra are found to decrease in the visible range.

3.4.2 Energy band gap (E_g)

The band gap energy (E_g) is achieved using the differential reflectance spectra, as depicted in Fig. 7. Thus, we can note an increase of E_g from 3.70 to 3.85 eV with Mn concentration increment which may be attributed to the optical scattering caused by grain boundaries and aggregates [21]. The obtained results are summarized in Table 2. It is worth noting that the estimated values show satisfactory agreement with previous work [22].

3.4.3 Refractive index and extinction coefficient

The refractive index is determined using the envelope method [23]:

$$n = \left[N + (N^2 - n_0^2 n_s^2)^{\frac{1}{2}} \right]^{\frac{1}{2}} \tag{3}$$

$$N = 2n_0 n_s \frac{T_M - T_m}{T_M T_m} + \frac{n_0^2 + n_s^2}{2} \tag{4}$$

where *n* is the refractive index of the ZnS:Mn thin films, *n*₀ and *n*_{*s*} are the refractive indices of air and glass substrate, respectively. *T*_{*M*} and *T*_{*m*} are the values of the envelope of the maximum and minimum positions of the transmittance spectra, respectively.

The dependence of the refractive index (*n*) on the wavelength of ZnS:Mn films is shown in Fig. 8. As it can be seen from this figure, *n* decreases with the increasing of wavelength which is in good agreement with transmittance

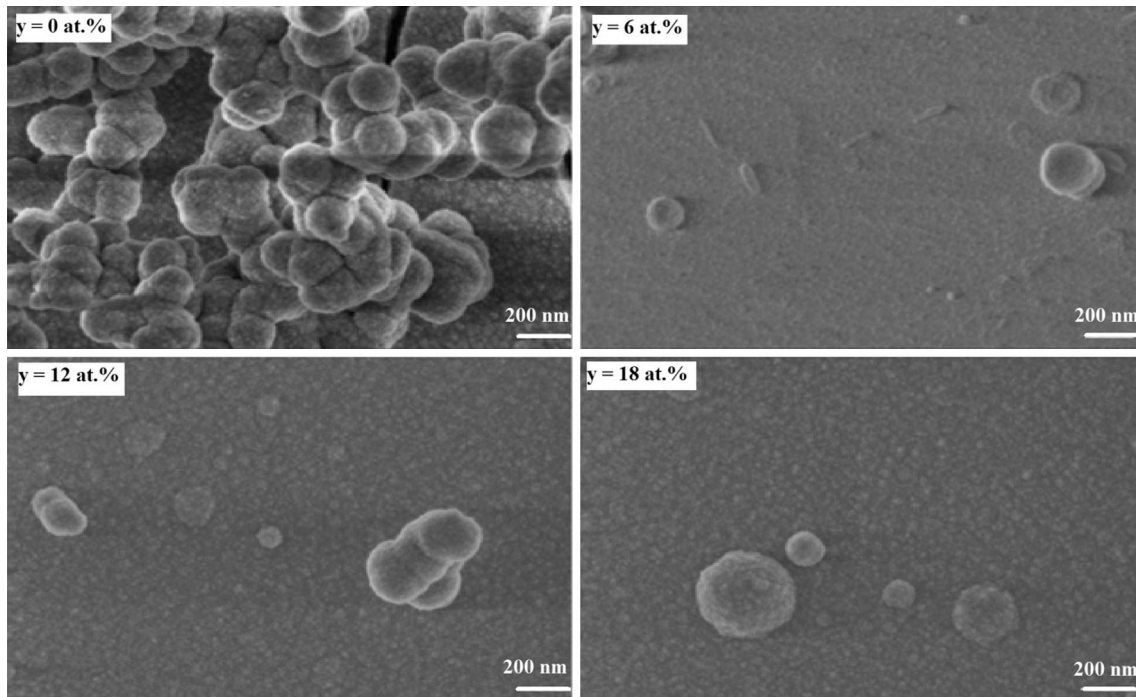


Fig. 4 SEM micrographs of ZnS:Mn thin films for various doping ratios

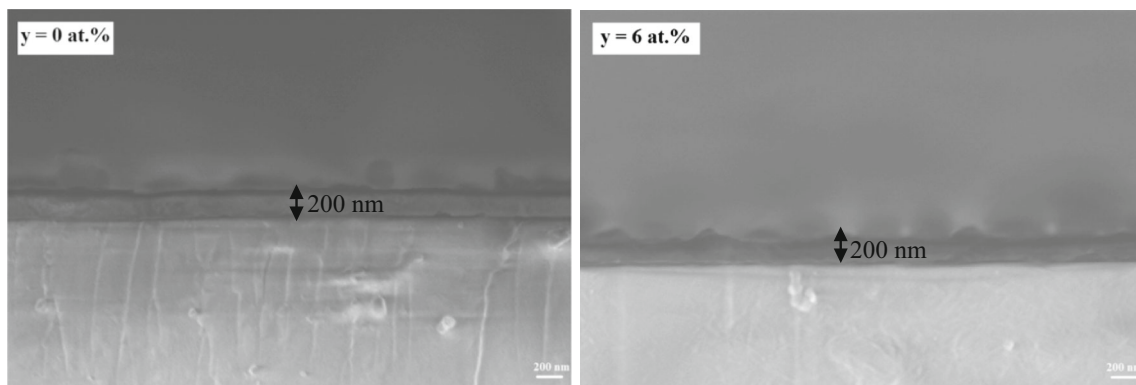


Fig. 5 Cross-sectional SEM micrographs of undoped and ZnS: (6 at. % Mn) thin films

values. Moreover, n decreases significantly when the Mn concentration increases from 0 to 6 at. % reaching 1.65 at $\lambda \geq 1000$ nm then, this value increases slightly to reach 1.69 with further increase of Mn concentration.

The estimated thickness (t) of the films is determined using the following relation [23]:

$$t = \frac{M\lambda_1\lambda_2}{2(\lambda_2n_1 - \lambda_1n_2)} \quad (5)$$

where M is the number of oscillations between the two extrema ($M = 1$ between two consecutive maxima or minima), λ_1 , n_1 and λ_2 , n_2 are the corresponding wavelengths and refraction indices [23].

The average thickness of ZnS:Mn thin films is about 199 nm. This value match very well with that obtained from the cross-sectional SEM micrographs (Fig. 5).

The extinction coefficient (k) in the transparency region can be obtained according to the following expression [24]:

$$k = \frac{\alpha\lambda}{4\pi} \quad (6)$$

where α is the absorption coefficient deduced from the formula given bellow [25]:

$$\alpha = \frac{1}{t} \ln \left(\frac{(1-R)^2}{T} \right) \quad (7)$$

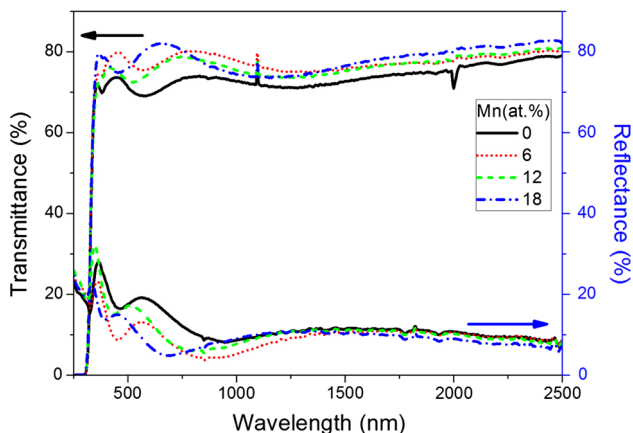


Fig. 6 Optical transmittance and reflectance spectra of ZnS:Mn thin films

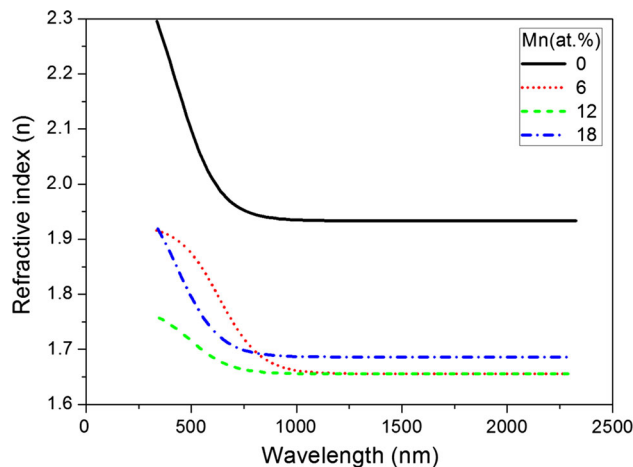


Fig. 8 Variation of refractive index (n) of ZnS:Mn thin films for different Mn concentrations

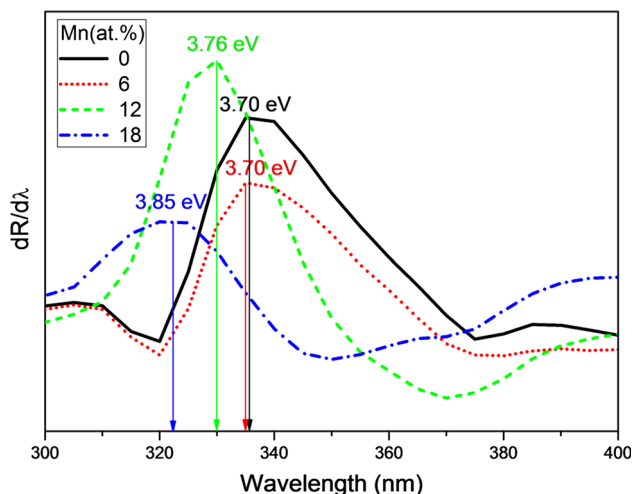


Fig. 7 Plots of $\frac{dR}{d\lambda}$ versus λ for manganese doped ZnS thin films

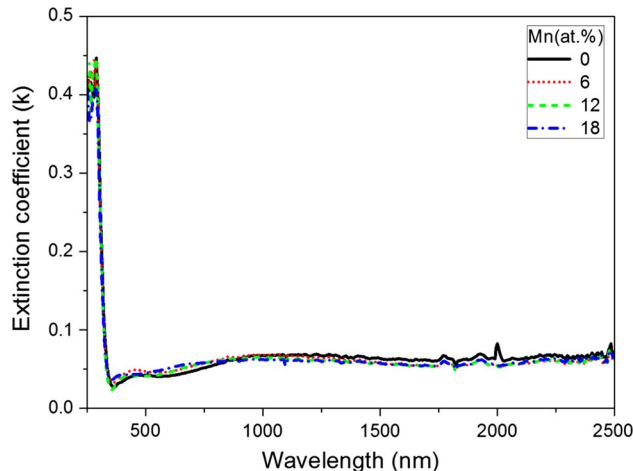


Fig. 9 Variation of extinction coefficient (k) of ZnS:Mn thin films for different Mn concentrations

Table 2 The estimated values of band gap energy (E_g and E_g^{PL}) and thickness (t) for manganese doped ZnS thin films

y (at. %)	E_g (eV)	E_g^{PL} (eV)	t (nm)
0	3.70	3.35	199
6	3.70	3.37	224
12	3.76	3.39	239
18	3.85	3.43	193

Figure 9 displays the dependence of the extinction coefficient on wavelength. It is found that k does not exceed 0.08 in the transparency region, which is a low value revealing the surface smoothness as well as the film homogeneity of ZnS:Mn layers.

3.4.4 Refractive index dispersion analysis

The dispersion of the refractive index (n) is evaluated according to the single oscillator model proposed by Wemple and DiDomenico [26], as shown in Fig. 10. According to this model, n can be described by the following expression [26]:

$$n^2(h\nu) = 1 + \frac{E_0 E_d}{E_0^2 - (h\nu)^2} \tag{8}$$

The oscillator energy E_0 and the interband optical strength E_d is related to the moments of optical dispersion M_{-1} and M_{-3} by the relations [27]:

$$M_{-1} = \frac{E_d}{E_0} \tag{9}$$

$$M_{-3} = \frac{E_d}{E_0^3} \tag{10}$$

The calculated values of E_0 , E_d , M_{-1} and M_{-3} , ϵ_∞ as well as $n(0)$ of ZnS:Mn thin films are listed in Table 3.

For further optical analysis, the contribution from the free carrier electric susceptibility (χ_e) to the real dielectric constant (ϵ_r) (Fig. 11) is discussed according to the Spitzer-Fan model [28]:

$$\epsilon_r = n^2 - k^2 = \epsilon_\infty - \left[\frac{e^2}{\pi c^2} \right] \left(\frac{N}{m^*} \right) \lambda^2 \tag{11}$$

$$\left[\frac{e^2}{\pi c^2} \right] \left(\frac{N}{m^*} \right) \lambda^2 = -4\pi\chi_e \tag{12}$$

where ϵ_∞ is the high frequency dielectric constant in the absence of any contribution from free carrier, $\frac{N}{m^*}$ is the carrier concentration to the effective mass ratio, e is the electronic charge and c is the light velocity.

According to Drude model, the plasma frequency (w_p) is related to the free charge carrier density, N , by the following equation [29]:

$$w_p = \left(\frac{e^2 N}{\pi c^2 m^*} \right)^{\frac{1}{2}} \tag{13}$$

The calculated values of w_p are tabulated in Table 3.

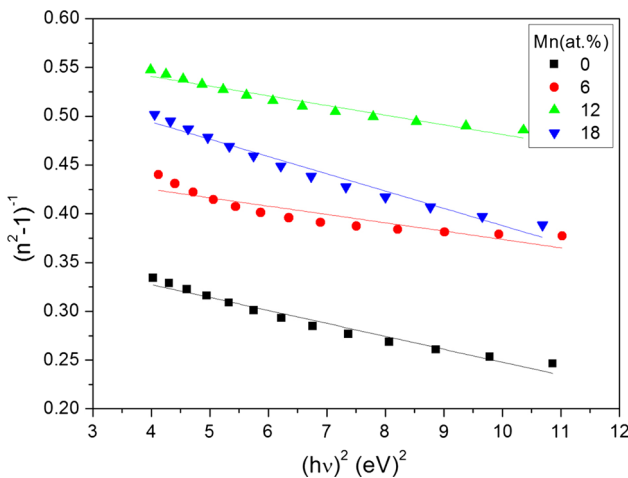


Fig. 10 A plot of $(n^2 - 1)^{-1}$ versus photon energy squared $(hv)^2$ of ZnS:Mn thin films

The variation of $-4\pi\chi_e$ versus λ^2 is presented in Fig. 12, we note that $-\chi_e$ becomes sufficiently large to reduce the dielectric constant $\epsilon_r(\lambda)$ as well as the refractive index $n(\lambda)$ in the infrared (IR) region.

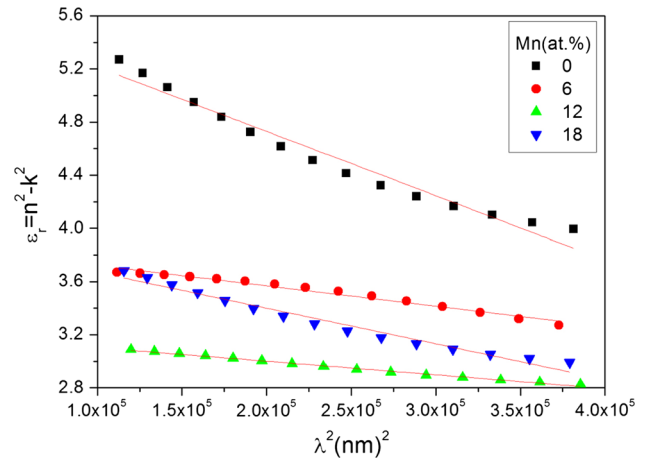


Fig. 11 Plots of optical dielectric constant $\epsilon_r = n^2 - k^2$ versus wavelength squared λ^2 for ZnS:Mn thin films for various Mn concentrations

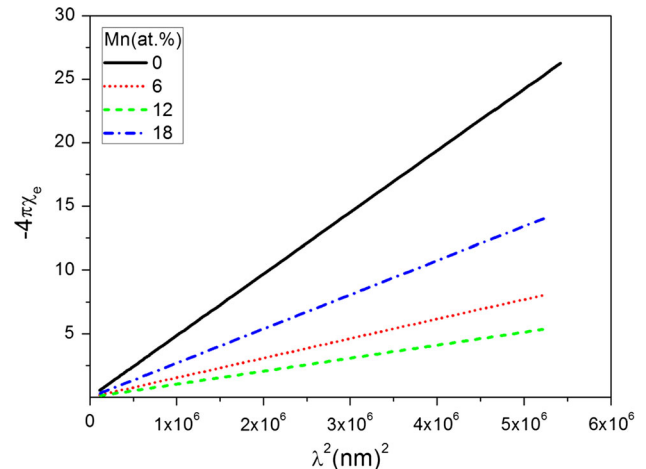


Fig. 12 Plots of $(-4\pi\chi_e)$ versus wavelength squared λ^2 of ZnS:Mn thin films

Table 3 Estimated values of optical parameters for manganese doped ZnS thin films

y (at. %)	E_0 (eV)	E_d (eV)	f (eV ²)	M_{-1}	M_{-3} (eV ⁻²)	$N/m^*(10^{49} \text{kg.cm}^{-3})$	n (0)	ϵ^{W-D}	ϵ^{S-F}	w_p (10 ⁴ cm ⁻¹)
0	5.35	14.07	75.27	2.63	0.09	5.35	2.39	5.70	5.33	22.01
6	7.33	15.97	117.06	2.18	0.04	1.70	1.97	3.88	3.90	12.40
12	7.65	13.18	100.83	1.72	0.03	1.13	1.79	3.21	3.82	10.11
18	6.10	10.99	67.04	1.80	0.05	2.96	1.98	3.94	3.19	16.39

Both ϵ_{∞}^{W-D} and ϵ_{∞}^{S-F} values obtained from Wemple–DiDomenico and Spitzer-Fan models, respectively, show a good satisfactory. These values are found to be very close to those obtained by Farag et al. [27].

The single oscillator parameters E_0 and E_d can be used for the determination of the third-order non-linear optical susceptibility $\chi^{(3)}$, which is a significant factor indicating whether the films are suitable for optical switching and photonic devices. It can be calculated by using the following relation [27, 30]:

$$\chi^{(3)} = A(\chi^{(1)})^4 = \frac{A}{(4\pi)^4}(n^2 - 1)^4 \tag{14}$$

$$\chi^{(3)} = A \left[\frac{E_0 E_d}{4\pi(E_0^2 - (h\nu)^2)} \right]^4 \tag{15}$$

where $A = 1.7 \times 10^{-10} \text{esu}$ and $\chi^{(1)}$ is the linear optical susceptibility.

The spectral dependence of $\chi^{(3)}$ with photon energy is displayed in Fig. 13. As seen, $\chi^{(3)}$ reaches its maximum at higher energy. This result is in good agreement with that reported by Abdolazadeh Ziabari et al. [30].

3.4.5 Photoluminescence studies

Photoluminescence (PL) spectroscopy is a non destructive technique for the study of structure, band gap, impurity

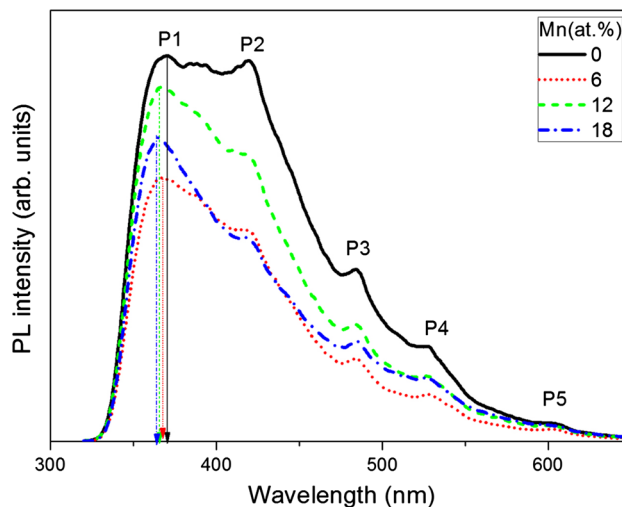


Fig. 14 Room-temperature photoluminescence (RT-PL) spectra of ZnS:Mn thin films excited at 300 nm

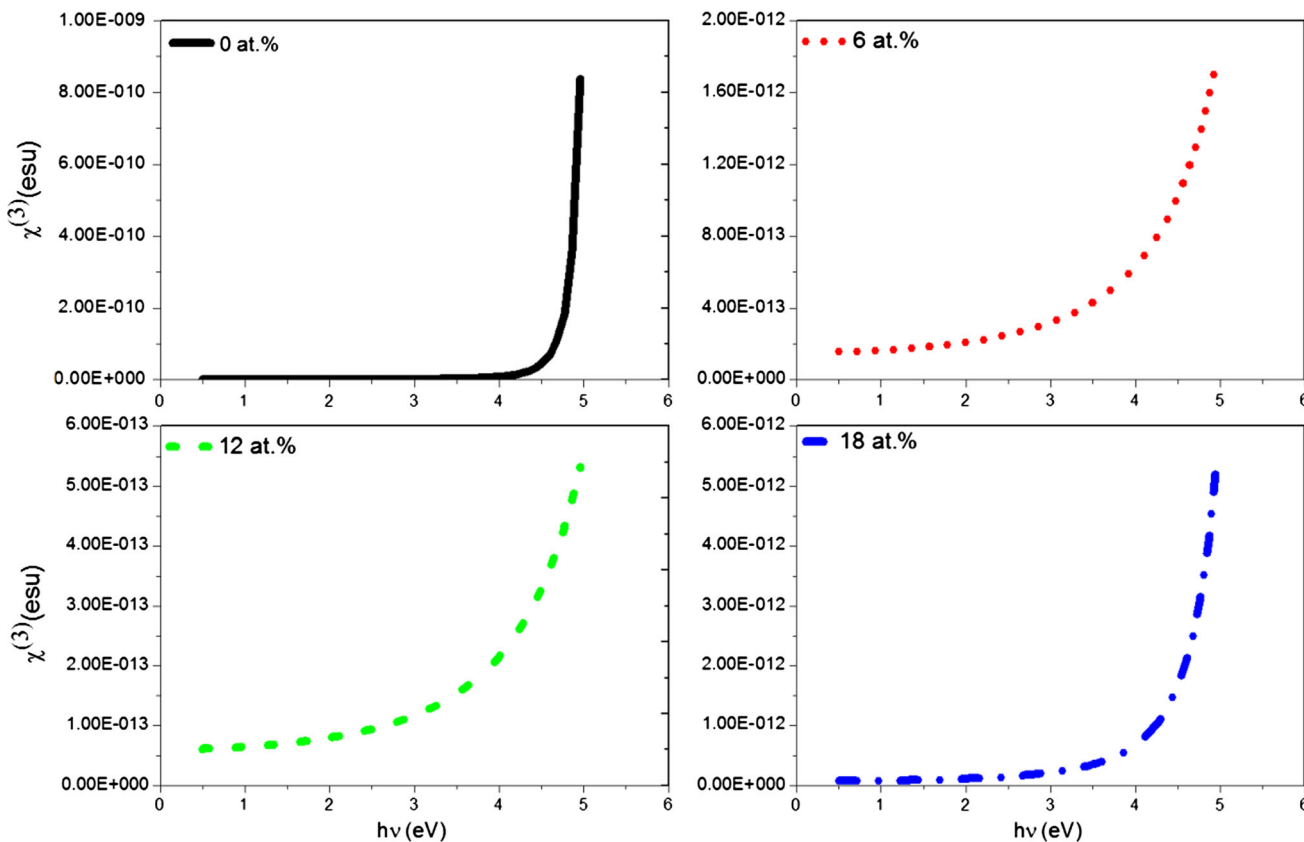


Fig. 13 Spectral dependence of third order non-linear susceptibility ($\chi^{(3)}$) of ZnS:Mn thin films

Table 4 Electrical parameters for manganese doped ZnS thin films

y (at. %)	Resistivity, ρ ($10^4 \Omega \cdot \text{cm}$)	Volume carrier concentration, N_v (10^{11} cm^{-3})	Surface carrier concentration, N_s (10^6 cm^{-2})	Hall mobility, μ ($10^1 \text{ cm}^2 \text{ V}^{-1} \text{ s}^{-1}$)	Free path, l (10^{-39} \AA)	$T_{(\lambda=550\text{nm})}(\%)$	Sheet resistance, R_s ($10^9 \Omega/\square$)	Figure of merit, Φ ($10^{-11} \Omega^{-1}$)
0	7.586	1.472	2.944	55.90	15.409	71	3.793	0.645
6	6.819	11.950	23.89	7.663	4.2455	78	3.409	1.652
12	8.834	9.784	19.57	7.222	3.7431	75	4.417	0.973
18	16.73	3.751	7.502	9.948	3.7456	79	8.365	0.997

levels as well as localized defects in semiconductor thin films [31]. The room temperature photoluminescence (RT-PL) spectra are recorded for ZnS thin films excited at 300 nm in the spectral range of 300–900 nm, as depicted in Fig. 14. The main peak, located at 365 nm (P1), may be due to the near band edge transitions (the band gap). Thus, we can note a difference between the band gap energy estimated from the PL spectra (E_g^{PL}) and the band gap energy calculated from the differential reflectance spectra (E_g) which is attributed to the difference in the momentum selection rule between the luminescence and absorption [29, 32]. The blue emission located at 420 nm and labeled P2, is associated with zinc vacancies V_{Zn} [33]. The observed luminescence at 484 nm labeled P3 is associated with zinc interstitials I_{Zn} [33]. However, two additional peaks are also observed at around 528 nm (P4) and 600 nm (P5). These emissions may be related to the sulfur vacancies V_{S} and sulfur interstitials I_{S} .

3.5 Electrical properties

In order to examine the effect of Mn doping on the electrical properties of ZnS thin films, Hall effect measurements are performed and the obtained results are summarized in Table 4. In fact, the n-type electrical conductivity is observed for all the samples. The resistivity value, is found to decrease slightly with Mn content increment up to 6 at. % and reach a minimum value of $6.819 \times 10^4 \Omega \cdot \text{cm}$. Then, it starts to increase with further increase of Mn content. The mean free path (l) of films is determined by the following equation [34]:

$$l = \left(\frac{h}{2e}\right) \left(\frac{3N}{\pi}\right)^{\frac{1}{3}} \mu \quad (16)$$

where h , e , N and μ are Plank's constant, electron charge, carrier concentration and mobility, respectively. The calculated l values are tabulated in Table 4. As seen, the free path values are lower than the crystallite size values calculated from XRD analysis (Table 1). Consequently, ionized impurity and structural defect scattering centers would be more dominant in scattering mechanisms than grain boundaries [34].

The figure of merit is employed to compare the performance of the grown ZnS films doped with Mn ions. The most common figure of merit formula is described by the following Haacke formula [34]:

$$\Phi = \frac{T^{10}}{R_s} \quad (17)$$

where T and R_s are the average transmittance at 550 nm wavelength and sheet resistance, respectively. Φ values are, also, presented in Table 4. The results indicate that ZnS: (6 at. % Mn) thin films exhibits the highest figure of merit among all the prepared samples, which reflects the good optoelectronic performance of this film.

4 Conclusion

ZnS:Mn thin films were successfully deposited on ordinary glass substrates by chemical bath deposition technique. According to XRD study, ZnS:Mn thin films showed poorly cubic crystalline structure. The crystallite size became larger by increasing the Mn amount up to 6 at. % reaching a maximum value of about 47.99 nm. Then, it decreased to 41.72 nm with further increase of Mn amount. The FTIR spectra of ZnS:Mn films did not reveal any band related to the vibrational modes of Mn. Furthermore, the inclusion of Mn ions in the ZnS matrix induced modifications to the surface morphology of the films by showing disappearance of agglomerates and amelioration of the surface homogeneity. Furthermore, the average thickness calculated from envelope method matched very well with the values estimated using cross-sectional SEM micrographs. Moreover, the optical study showed a significant enhancement of the transmittance after Mn doping. Electrical study showed that the minimum of resistivity is obtained for 6 at. % Mn doping concentration.

References

1. H. Lekiket, M.S. Aida, Chemical bath deposition of nanocrystalline ZnS thin films: influence of pH on the reaction solution. Mater. Sci. Semicond. Process. **16**, 1753–1758 (2013)

2. G.L. Agawane, S.W. Shin, M.S. Kim, M.P. Suryawanshi, K.V. Gurav, A.V. Moholkar et al., Green route fast synthesis and characterization of chemical bath deposited nanocrystalline ZnS buffer layers. *Curr. Appl. Phys.* **13**, 850–856 (2013)
3. D.Y. Yang, S.-M. Lee, W.J. Jang, K.C. Choi, Flexible organic light-emitting diodes with ZnS/Ag/ZnO/Ag/WO₃ multilayer electrode as a transparent anode. *Org. Electron.* **15**, 2468–2475 (2014)
4. X. Ye, Y. Li, J. Dong, J. Xiao, Y. Ma, L. Qi, Facile synthesis of ZnS nanobowl arrays and their applications as 2D photonic crystal sensors. *J. Mater. Chem. C* **1**, 6112 (2013)
5. L. Hu, F. Chen, P. Hu, L. Zou, X. Hu, Hydrothermal synthesis of SnO₂/ZnS nanocomposite as a photocatalyst for degradation of Rhodamine B under simulated and natural sunlight. *J. Mol. Catal. A: Chem.* **411**, 203–213 (2016)
6. Y. Chen, L. Zhang, J. Zhang, P. Liu, T. Zhou, H. Zhang et al., Fabrication of transparent ZnS ceramic by optimizing the heating rate in spark plasma sintering process. *Opt. Mater. (Amst)* **50**, 36–39 (2015)
7. M.M. Islam, S. Ishizuka, A. Yamada, K. Sakurai, S. Niki, T. Sakurai et al., CIGS solar cell with MBE-grown ZnS buffer layer. *Sol. Energy Mater. Sol. Cell.* **93**, 970–972 (2009)
8. J. Cui, X. Zeng, M. Zhou, C. Hu, W. Zhang, J. Lu, Tunable blue and orange emissions of ZnS: Mn thin films deposited on GaN substrates by pulsed laser deposition. *J. Lumin.* **147**, 310–315 (2014)
9. D. Kurbatov, A. Opanasyuk, S.M. Duvanov, A.G. Balogh, H. Khlyap, Growth kinetics and stoichiometry of ZnS films obtained by close-spaced vacuum sublimation technique. *Solid State Sci.* **13**, 1068–1071 (2011)
10. V.L. Gayou, B. Salazar-Hernandez, M.E. Constantino, E.R. Andrés, T. Díaz, R.D. Macuil et al., Structural studies of ZnS thin films grown on GaAs by RF magnetron sputtering. *Vacuum* **84**, 1191–1194 (2010)
11. V.G. Bessergenev, E.N. Ivanova, Y.A. Kovalevskaya, S.A. Gromilov, V.N. Kirichenko, S.M. Zemskova et al., Optical and structural properties of ZnS and ZnS: Mn films prepared by CVD method. *Mater. Res. Bull.* **30**, 1393–1400 (1995)
12. S. Ummartyotin, Y. Infahsaeng, A comprehensive review on ZnS: from synthesis to an approach on solar cell. *Renew. Sustain. Energy Rev.* **55**, 17–24 (2016)
13. K.B. Bacha, A. Timoumi, N. Bitri, H. Bouzouita, Structural, morphological and optical properties of sprayed ZnS thin films on various substrate natures. *Opt. - Int. J. Light Electron Opt.* **126**, 3020–3024 (2015)
14. A. Ates, M.A. Yıldırım, M. Kundakçı, A. Astam, Annealing and light effect on optical and electrical properties of ZnS thin films grown with the SILAR method. *Mater. Sci. Semicond. Process.* **10**, 281–286 (2007)
15. N. Arbi, I.B. Assaker, M. Gannouni, A. Kriaa, R. Chtourou, Experimental investigation of the effect of Zn/S molar ratios on the physical and electrochemical properties of ZnS thin films. *Mater. Sci. Semicond. Process.* **40**, 873–878 (2015)
16. A. Jrad, T. Ben, Nasr, N. Turki-Kamoun, Effects of Al content on physical properties of ZnS thin films prepared by chemical bath deposition. *J. Mater. Sci.: Mater. Electron.* **26**, 8854–8862 (2015)
17. R.K. Chandrakar, R.N. Baghel, V.K. Chandra, B.P. Chandra, Synthesis, characterization and photoluminescence studies of Mn doped ZnS nanoparticles. *Superlattices Microstruct.* **86**, 256–269 (2015)
18. A.A. Ortiz-Hernández, V.H.M. García, M.L.P. Arrieta, J.J.O. Sigala, J.D.J.A. Ibarra, H.R. Vega-Carrillo et al., Thermoluminescent properties of ZnS: Mn nanocrystalline powders. *Appl. Radiat. Isot.* **99**, 105–109 (2015)
19. S. Muthukumaran, M. Ashok kumar, Structural, FTIR and photoluminescence properties of ZnS: Cu thin films by chemical bath deposition method. *Mater. Lett.* **93**, 223–225 (2013)
20. C. Chlique, O. Merdrignac-conanec, N. Hakmeh, X. Zhang, J. Adam, Transparent ZnS Ceramics by Sintering of High Purity Monodisperse **3074**, 3070–3074 (2013)
21. T. Kucukomeroglu, E. Bacaksiz, C. Terzioglu, A. Varilci, Influence of fluorine doping on structural, electrical and optical properties of spray pyrolysis ZnS films. *Thin Solid Films* **516**, 2913–2916 (2008)
22. A. Goudarzi, G.M. Aval, S.S. Park, M. Choi, R. Sahraei, M.H. Ullah et al., Low-temperature growth of nanocrystalline Mn-doped ZnS thin films prepared by chemical bath deposition and optical properties. *Chem. Mater.* **21**, 2375–2385 (2009)
23. J.C. Manifacier, J. Gasiot, J.P. Fillard, Simple Method for the Determination of the Optical Constants. *J. Phys. E* **9**, 1002–1004 (1976)
24. A. Arunachalam, S. Dhanapandian, C. Manoharan, G. Sivakumar, Physical properties of Zn doped TiO₂ thin films with spray pyrolysis technique and its effects in antibacterial activity. *Spectrochim. Acta. A. Mol. Biomol. Spectrosc.* **138**, 105–112 (2015)
25. A. Mhamdi, R. Mimouni, A. Amlouk, M. Amlouk, S. Belgacem, Study of copper doping effects on structural, optical and electrical properties of sprayed ZnO thin films. *J. Alloys Compd.* **610**, 250–257 (2014)
26. S.H. Wemple, M. DiDomenico, Behavior of the Electronic Dielectric Constant in Covalent and Ionic Materials. *Phys. Rev. B* **3**, 1338–1351 (1971)
27. A.A.M. Farag, M.A. Rafea, N. Roushdy, O. El-Shazly, E.F. El-Wahidy, Influence of Cd-content on structural and optical dispersion characteristics of nanocrystalline Zn 1– xCd_x films. *J. Alloys Compd.* **621**, 434–440 (2015)
28. W.G. Spitzer, H.Y. Fan, Determination of Optical Constants and Carrier Effective Mass of Semiconductors. *Phys. Rev.* **106**, 882–890 (1957)
29. A.M. Al-Baradi, M.M. El-Nahass, M.M.A. El-Raheem, A.A. Atta, A.M. Hassanien, Effect of gamma irradiation on structural and optical properties of Cd₂SnO₄ thin films deposited by DC sputtering technique. *Radiat. Phys. Chem.* **103**, 227–233 (2014)
30. A.A. Ziabari, F.E. Ghodsi, Effects of the Cd:Zn: S molar ratio and heat treatment on the optical and photoluminescence properties of nanocrystalline CdZnS thin films. *Mater. Sci. Semicond. Process.* **16**, 1629–1636 (2013)
31. A.D. Yoffe, Low-dimensional systems: quantum size effects and electronic properties of semiconductor microcrystallites (zero-dimensional systems) and some quasi-two-dimensional systems. *Adv. Phys.* **42**, 173–262 (1993)
32. S.R. Meher, A. Subrahmanyam, M.K. Jain, Composition-dependent structural, optical and electrical properties of In_xGa_{1–x}N (0.5 ≤ x ≤ 0.93) thin films grown by modified activated reactive evaporation. *J. Mater. Sci.* **48**, 1196–1204 (2012)
33. P. Prathap, N. Revathi, Y.P.V. Subbaiah, K.T.R. Reddy, R.W. Miles, Preparation and characterization of transparent conducting ZnS: Al films. *Solid State Sci.* **11**, 224–232 (2009)
34. G. Turgut, E. Sonmez, S. Duman, Evaluation of an Nd doping effect on characteristic properties of tin oxide. *Mater. Sci. Semicond. Process.* **30**, 233–241 (2015)